Data processing method for experimental studies of deformation in a rock sample under uniaxial compression

Andrei Golosov[1*], *Olga* Lubimova[2], *Mikhail* Zhevora[2], *Vladislava* Markevich[2] and *Vladimir* Siskov[2]

[1]Department of Mining and Integrated Development of Geo-resources, School of Engineering, Far Eastern Federal University, Vladivostok, Russia.
[2]Department of Mechanics and Mathematical Modeling, School of Engineering Far Eastern Federal University, Vladivostok, Russia.

Abstract. As a result of experimental and theoretical studies, the patterns of behavior of rocks in a condition close to destructive are the focal nature of the preparation of macrocracking, which allowed us to include the mesocrack structure of the material, which is the main element in the preparation of macrocracking. Differences in this new approach to mathematical modeling will let adequately describe dissipative mesocrack structures of various hierarchical levels of geodesy, predict dynamic changes, structures and mechanical properties of both rock samples and massif, which also lead to resource-intensive experimental studies. In this paper, with usage of the methods of cluster, factor, and statistical analysis, we set the task of processing the data of experimental studies of the laws of deformation and preparing macro-fracture of rock samples by various methods, including acoustic and deformation observations.

1 Introduction

The task of processing experimental data obtained by the combined method of deformation-acoustic studies of samples of compressed rocks by machine learning methods [1-2]. Considering that the characteristics of the model should be variable and adapt to changing conditions, an approach that is related to the development of the concept of multilayer neural networks (neural networks, NN) with training using the back propagation (BP) method is promising. Modern machine learning methods (Machine Learning Techniques, MLT) have already found their use, including in modeling the mechanical characteristics of rock samples, which consists in carrying out a number of studies to determine the uniaxial compression strength (σ_c) of individual types of granite, with such input data as free

* Corresponding author: a-dune@mail.ru

porosity (N48), bulk density in the dry state (d) and ultrasound velocity (v). Studies are related to the selection of the most effective model among adaptive digital filters, a neural network, and autoregressive analysis [3-8]. Experimental data for neural network modeling should be pre-analyzed and processed. Moreover, taking into account the originality of the approach to the deformation-acoustic method for isolating the localization of the defect center, it is necessary to identify methods that allow the most efficient description of the data obtained from the general approaches to processing experimental data.

The aim of this work was to process the results of experimental data using methods of cluster analysis and factor analysis to identify sensors in the focal and near focal areas. Statistical processing of data of the largest cluster for the application of experimental results in mathematical modeling.

2 A brief description of the experiment

To develop a comprehensive method for reliable determination of the system of deformation precursors of fracture of rock samples under uniaxial compression, a cylindrical rock sample was studied. The bases of this sample are flat, parallel to each other and perpendicular to the lateral surface of the cylinder. Height is 108 mm, diameter is 54 mm

Examination of the sample has been carried out on a servo-controlled hydraulic rigid press MTS-816 using a ball bearing in the loading device (figure 1).

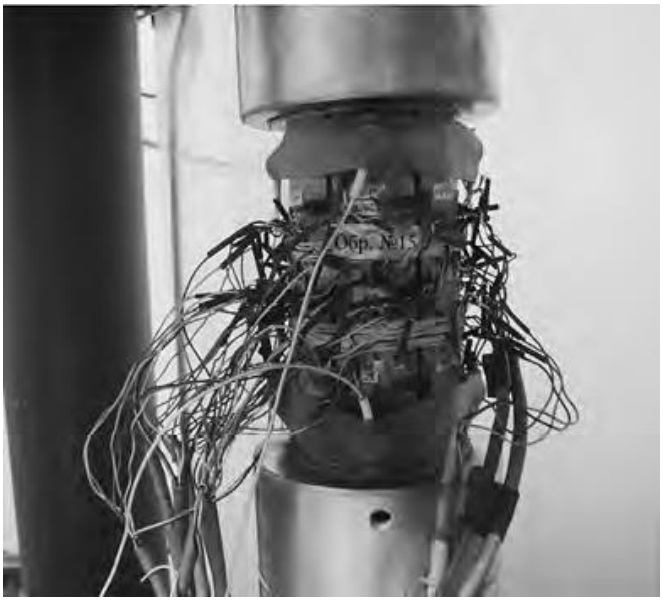

Fig. 1. The sample before the test.

Sensors for measuring longitudinal and transverse strains are located on the lateral surface of the sample in the central and in the end parts according to the diagram shown in figure 2.

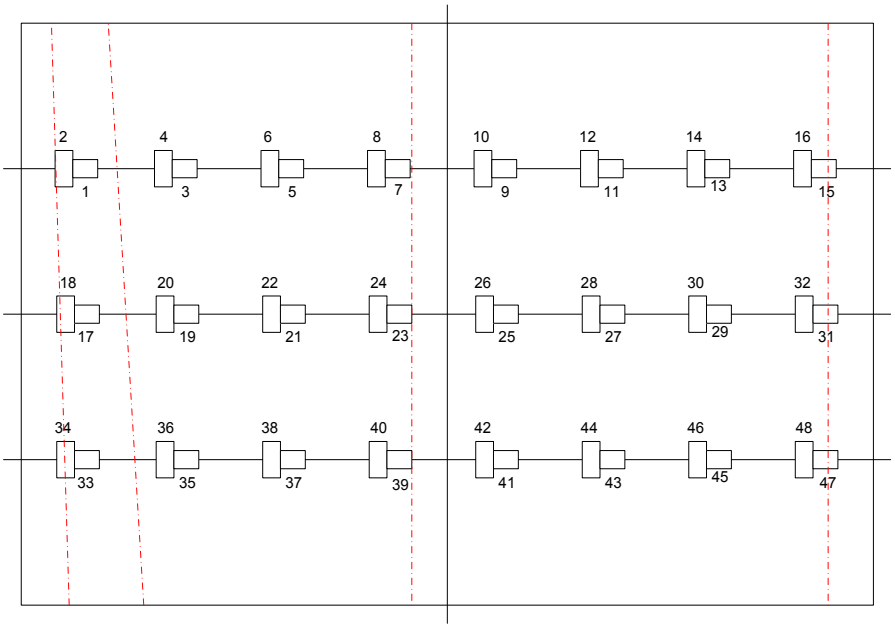

a)

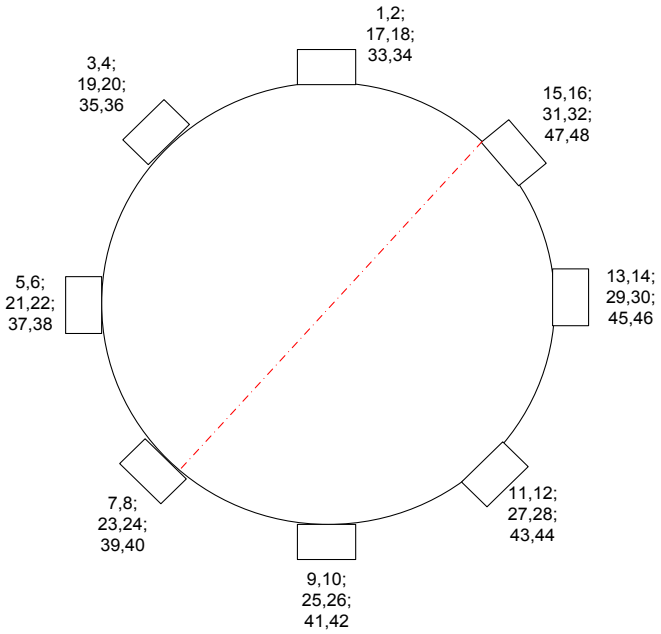

b)

Fig. 2. Positioning of the strain gauges: a) side view, b) top view.

Under uniaxial compression of the sample, strain gauges record changes in the corresponding deformations. Records are shown in Table 1. A detailed description of the experimental research methodology is described in [9].

Table 1. Data recorded by strain gages.

			Pair 17 (focal area)			
Stress (MPa)	Emission quantity per measurement interval	Cumulative emissions	Sensor 33	Sensor 34	Pair 17 - Poisson's Ratio	Pair 17 - modulus of elasticity
0	0	0	0	0	0	
0,1863487	0	0	0	0,003767	0	49,46461
0,6652691	0	0	0	0,011302	0	58,86327
1,2782431	0	0	0	0,011302	0	113,0994
1,6655245	0	0	-0,00376	0,007535	0,4990655	221,0494
1,893985	0	0	0	0,011302	0	167,5805
2,1607505	0	0	0	0,011302	0	191,184
2,3392952	0	0	0	0,007535	0	310,4726
2,5098683	0	0	0	0,007535	0	333,1112
2,6909596	0	0	0	0,015069	0	178,5729
2,8334122	0	0	-0,00376	0,015069	0,24953275	188,0261
2,9203304	0	0	-0,00376	0,015069	0,24953275	193,794
3,0594249	0	0	-0,00752	0,011302	0,66542066	270,6991

3 Data processing by cluster and factor analysis methods

The experimental data were processed as follows: the entire stress range (from 0 to 336 MPa) was divided into six different intervals with different step sizes. As the stress increased, the interval length and the step size decreased, for a more detailed examination of the state of the sample at the time of the appearance of anomalous behavior. So, for example, in the first interval (from 0 to 90 MPa), the step size is 10 MPa, and in the last (from 320 MPa to 336 MPa) - 2 MPa.

Preliminarily, pairs of strain gages were built on phase planes ε_z, ε_φ on each interval (figures 3 - 4).

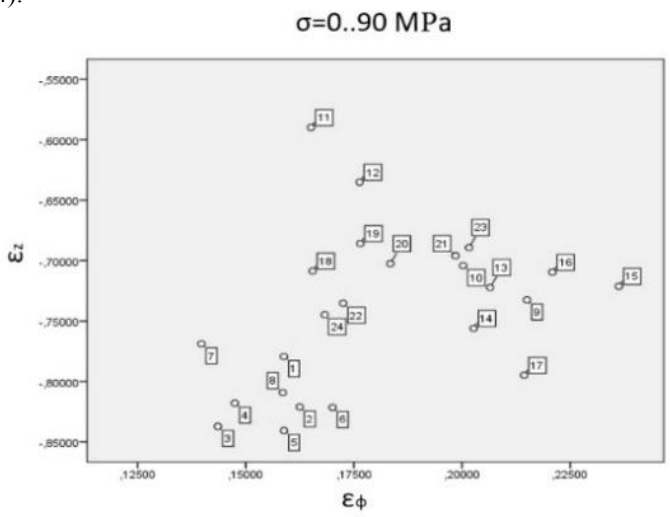

Fig. 3. Preliminary plotting of pairs of strain gauges on phase planes ε_z, ε_φ at the initial stage of loading.

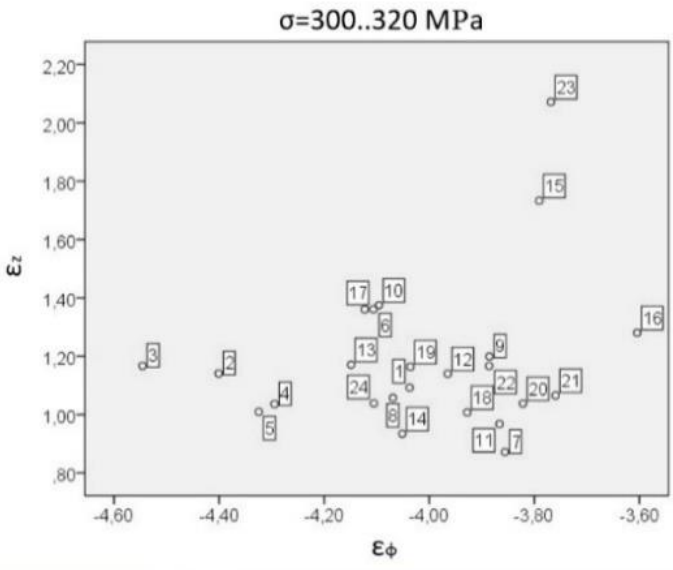

Fig. 4. Preliminary plotting of pairs of strain gauges on phase planes ε_z, ε_φ at the last stage of loading.

On the entire range of stresses (from 0 to 336 MPa), stress–strain diagrams were plotted. After that, three types of plots behavior were revealed (Fig. 5).

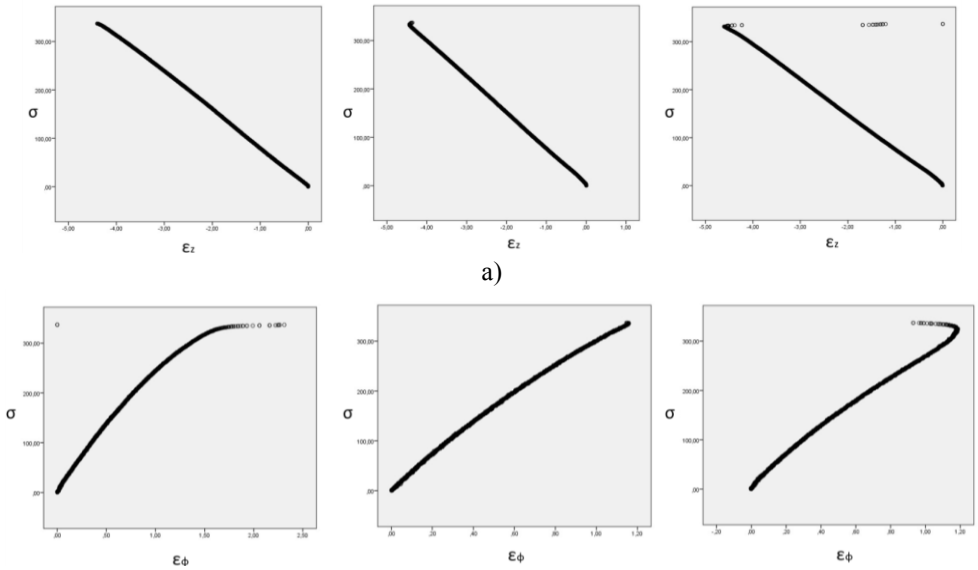

Fig. 5. Identification of anomalous behavior of the plots: a)plane (σ,ε_z), b)plane (σ,ε_φ).

The results were correlated with the sensors layout on the sample surface (Fig. 6).

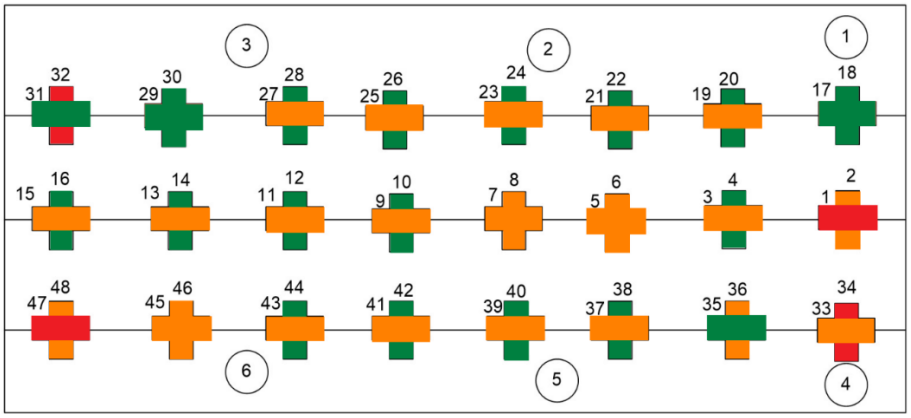

Fig. 6. Sensors layout with anomalies: red – noticable reverse deformations, orange – lesser reverse deformations, green – no reverse deformations.

According to figures 3 - 4 and figure 6, sensors with abnormal readings of reverse deformations are found in the places of fracture of the sample, which were revealed experimentally.

On the next step, centroid clustering was carried out with the measure of the square of Euclidean metric of the plane data (ε_z, ε_φ) to select the largest cluster for subsequent statistical processing, at each interval with the corresponding step. An example of clustering in the first and last section is shown in figure 7.

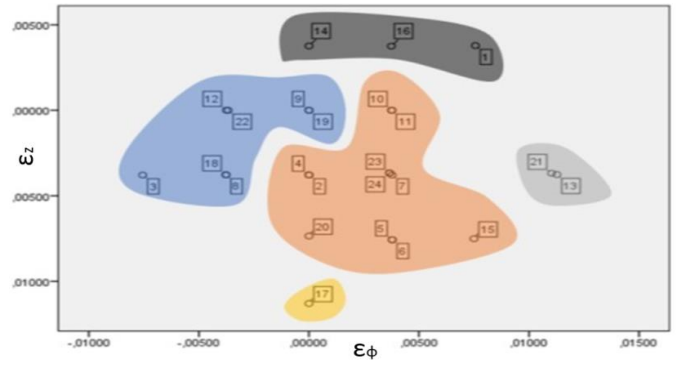

a)

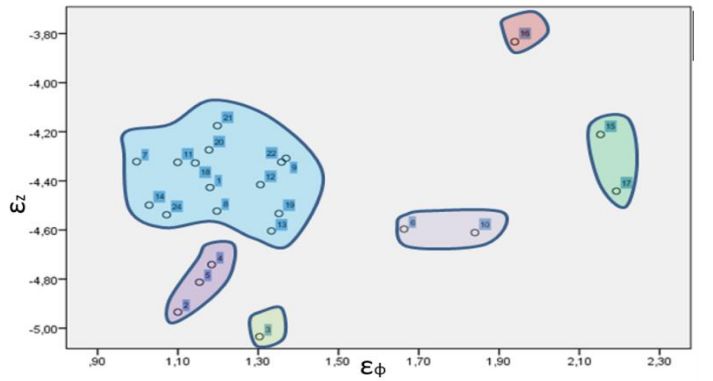

b)

Fig. 7. Clustering for stresses on interval: a) $\sigma_i \in$ [0-90] MPa, b) $\sigma_i \in$ [320-336] MPa.

Sensors, which on each interval always belong to the largest cluster, were identified and included into the Table 2.

Table 2. Sensors, which always belong to the largest cluster.

σ_i, MPa	0-90	90-171	171-260	260-300	300-320	320-336
Pair number	-	1, 13, 14, 24	1, 8, 24	1, 8, 9, 11, 12, 14, 18, 19, 20, 21, 22, 24	1, 7, 8, 9, 11, 12, 13, 14, 18, 19, 20, 21, 22, 24	1, 7, 8, 9, 11, 12, 13, 14, 18, 19, 20, 21, 22, 24

Statistical processing was carried out for the largest cluster, for each step of the fragmentation. The individual results of statistical processing are presented in Table 3, for the purpose of demonstration.

Table 3. An example of statistical processing completed.

	Transverse	Longitudinal
Average	1.200	-4.399
Standard error	0.033	0.033
Median	1.188	-4.371
Mode	-	-
Standard deviation	0.126	0.124
Dispersion	0.015	0.015
Excess	-1.247	-0.934
Asymmetry	-0.060	-0.034
Interval	0.372	0.428
Minimum	0.997	-4.604
Maximum	1.369	-4.175
Sum	16.810	-61.594
Amount	14	14

After carrying out the statistical processing, a graph of the relation between strain and stress with confidence intervals was plotted using the average values of ε_z and ε_φ of the largest cluster (figure 8).

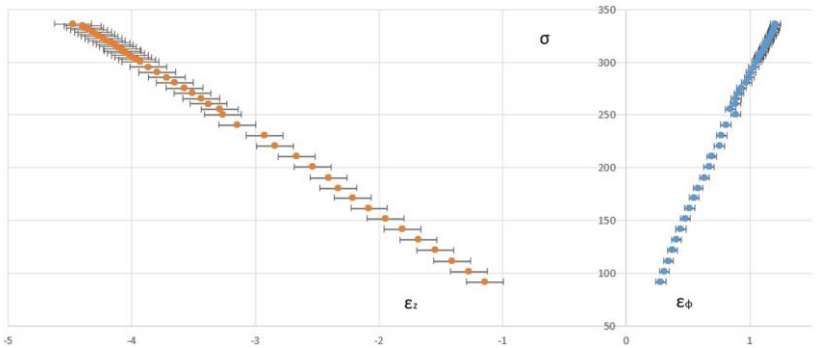

Fig. 8. Allocation of average strains of the largest cluster for the phase plane (ε_φ, ε_z) over the entire range of uniaxial compression

In addition, in the interval $\sigma_i \in [300\text{-}330]$ MPa with a step of 2 MPa, the Poisson's ratios for each pair of sensors were calculated. For some pairs of sensors, Poisson's ratio has the maximum allowable value (Table 4).

Table 4. An example of Poisson's ratios calculation result

Pair of sensors	ν	Pair of sensors	ν
1	0.269	13	0.280
2	0.258	14	0.231
3	0.254	15	0.455
4	0.241	16	0.353
5	0.232	17	0.328
6	0.327	18	0.256
7	0.226	19	0.285
8	0.259	20	0.272
9	0.308	21	0.283
10	0.335	22	0.298
11	0.249	23	0.542
12	0.284	24	0.251

Table 5. Results of cluster comparison for the phase plane (ε_φ, ε_z) and straight line (ν)

σ_i, MPa	**ε**	**ν**
300	1, 7, 8, 9, 11, 12, 13, 14, 18, 19, 20, 21, 22, 24	2, 3, 4, 5, 7, 8, 11, 14, 18, 24
302		2, 3, 4, 5, 7, 8, 11, 14, 18, 24
304		1, 2, 3, 4, 5, 7, 8, 11, 14, 18, 20, 24
306		2, 3, 4, 5, 7, 8, 11, 14, 18, 24
308		1, 2, 3, 4, 7, 8, 11, 12, 13, 18, 19, 20, 21, 24
310		2, 3, 4, 5, 7, 8, 11, 14, 18, 24
312		1, 9, 12, 13, 19, 20, 21, 22
314		1, 9, 12, 13, 19, 20, 21, 22
316		1, 9, 12, 13, 19, 20, 21, 22
318		2, 3, 4, 5, 7, 8, 11, 14, 18, 24
320		2, 3, 4, 5, 7, 8, 11, 14, 18, 24
322		2, 3, 4, 5, 7, 8, 11, 14, 18, 24
324		1, 2, 3, 4, 5, 7, 8, 11, 14, 18, 20, 24
326		2, 3, 4, 5, 7, 8, 11, 14, 18, 24
328		1, 2, 3, 4, 5, 7, 8, 11, 14, 18, 20, 24
330		1, 2, 3, 4, 5, 7, 8, 9, 11, 12, 13, 14, 18, 19, 20, 21, 22, 24
300-330		-

For the calculated values of the coefficients, centroid clustering was carried out with a Chebyshev distance as a measure. Then, the sensors, which belong to the largest cluster at each step, as well as throughout the interval were identified. The data obtained were correlated with the data from Table 4 and are shown in Table 5.

According to Table 5, there are no sensors, which belong to the largest cluster at all steps. Therefore, statistical processing was carried out for each step (Table 6), and then, with the average values of the Poisson's ratio at each step, a graph of the realtion between Poisson's ratios and stresses was plottted (figure 9).

Table 6. An example of statistical processing for the Poisson's ratio.

Average	0.284
Standard error	0.010
Median	0.272
Mode	-
Standard deviation	0.051
Dispersion	0.002
Excess	4.549
Asymmetry	1.809
Interval	0.228
Minimum	0.226
Maximum	0.455
Sum	6.547
Amount	23

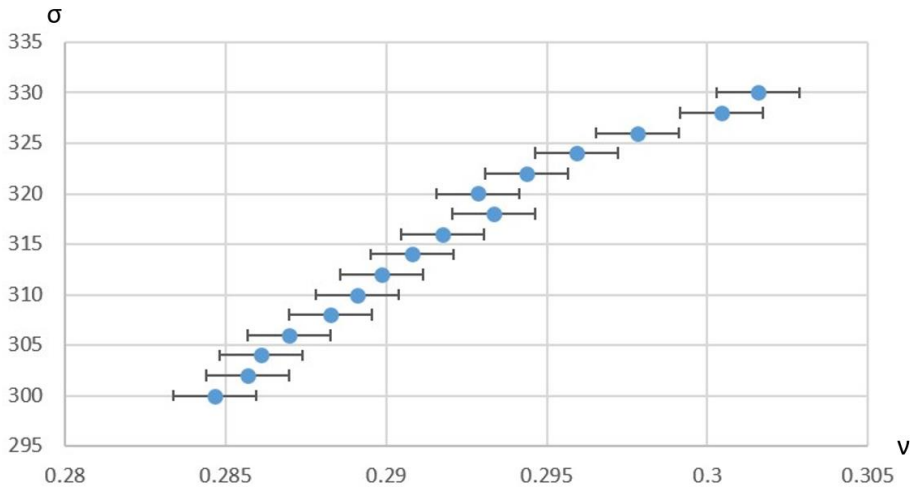

Fig. 9. Allocation of the average values of the Poisson's ratio in the interval $\sigma_i \in$ [300-330] MPa

The results of cluster analysis gave 5-6 groups of sensors. An unambiguous interpretation of the clusters is difficult. To clarify the interpretation of the results of cluster analysis, a factor analysis was carried out at the same intervals of stress values as for cluster analysis. The analysis was carried out separately for three sets of sensors: ε_φ sensors, ε_z sensors, for the entire group of sensors. Significant loads of the factor with values > 0.700 were considered. To rotate the factor matrix, the varimax method was used.

Additionally, the verification of the correctness of the choice of the border of 320 MPa was carried out. It is in the range of 320-336 MPa that one factor is divided into several factors. The verification was carried out for intervals of 310-336 MPa and 315-336 MPa. In both cases, factor analysis gave two factors, one of which contained only one to four sensors. Sensors on ε_φ (odd-numbered sensors) gave the following results: on the stress intervals 1,2,3,4,5, one factor is identified which contains all the points; on the interval 320-336 MPa, three factors are distinguished, see Tables 8 - 9. Three factors are distinguished in the interval 320-336, see Table 7.

Table 7. Factors at $\sigma_i \in$ [320-336] MPa.

Factor number	ε_φ sensor numbers, which belong to factor
F_1	3-13,21-31,35,37
F_2	17,19, 39-47
F_3	1,33

If instead of the interval 320-336 MPa we take 315-336 MPa, two factors stand out. See Table 7.

Table 8. Factors at $\sigma_i \in$ [315-336] MPa.

Factor number	ε_φ sensor numbers, which belong to factor
F_1	All other
F_2	3,19,33,47

Finally, if we take the interval 310-336 MPa, we have the following result

Table 9. Factors at $\sigma_i \in$ [310-336] MPa.

Factor number	ε_φ sensor numbers, which belong to factor
F_1	All other
F_2	3,33,47

Sensors according to ε_z (sensors with even numbers) give the following results: on the stress intervals 1, 2, 3, 4, 5, one factor is allocated that contains all the points; in the interval 320-336 MPa, two factors are distinguished, see Table 10.

Table 10. Factors at $\sigma_i \in$ [320-336] MPa.

Factor number	ε_z sensor numbers, which belong to factor
F_1	All other
F_2	2,4,20,34,48

If instead of the interval 320-336 MPa we take 315-336 MPa, two factors stand out:

Table 11. Factors at $\sigma_i \in$ [315-336] MPa.

Factor number	ε_z sensor numbers, which belong to factor
F_1	2-30,36-48
F_2	32,34

If instead of the interval 310-336 MPa, two factors stand out:

Table 12. Factors at $\sigma_i \in$ [310-336] MPa.

Factor number	ε_z sensor numbers, which belong to factor
F_1	All other
F_2	34

The use of data for all sensors (both ε_φ and ε_z) gives the following results: on the stress intervals 1, 2, 3, 4, 5, one factor is selected that contains all the points; in the interval 320-336 MPa, two factors are distinguished, see Table 13.

Table 13. Factors at $\sigma_i \in$ [320-336] MPa for all sensors.

Factor number	Sensor numbers, which belong to factor
F_1	All other
F_2	1,3,32,33,34,47

The fact that factors for different types of sensors combine sensors partially located in different places of the sample is most likely explained by the different nature of the deformations along the two selected axes. Results for three groups of sensors are shown in Table 14.

Table 14. Results of factor analysis for three group of sensors.

Factor number	Sensor numbers ε_φ, which belong to factor	Sensor numbers ε_z, which belong to factor	Numbers of all sensors, which belong to factor
A	All other	All other	All other
B	3,19,33,47	2,4,20,34,48	1,3,32,33,34,47

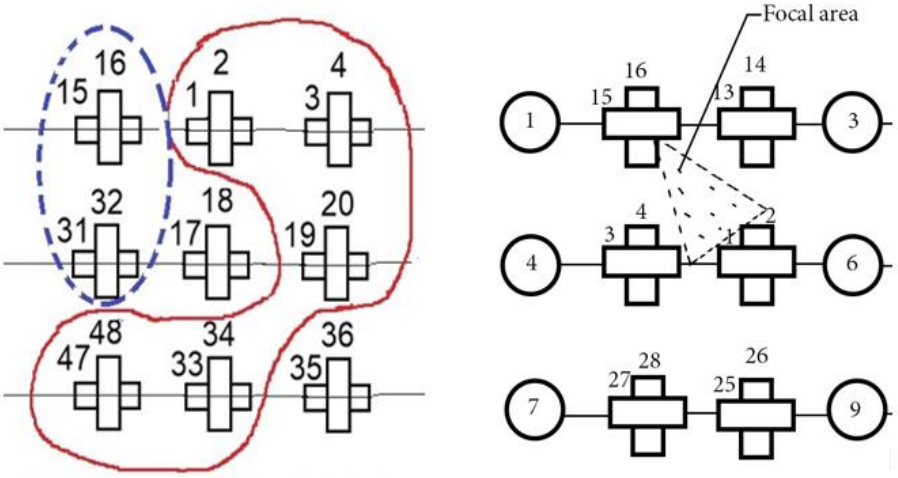

Fig. 10. Sensors that fall into the same clusters in several methods of rotation of the factor matrix: the sensors that fall into cluster B in 3 methods are highlighted in red; blue – in 1 and 2 methods (left), and experimentally discovered location of the destruction center (right).

.

4 Conclusions

With a certain degree of certainty, it can be argued that two factors mean dividing the set of sensors (and thereby local places on the sample) into two sets: A - “local places without features” and B - “local places with features, possibly focal or near focal ".

For the sample under study, set B most likely consists of pairs of sensors 1-2, 3-4, 19-20, 33-34, 47-48. Sensors that are found in at least two factor divisions are taken.

The data on the deformation of the specimen along the axes φ and z are not enough to confidently draw a conclusion about the location of the fracture site.

This work was presented at The 1st International Scientific Conference “Problems in Geomechanics of Highly Compressed Rock and Rock Massifs”.

This work was supported by a grant from the Ministry of Science and Higher Education. Unique Agreement Identifier is RFMEFI58418X0034.

References

1. M.A. Guzev, V.N. Odintsev, V.V. Makarov, Principals of geomechanics of highly stressed rock and rock massifs, 506 (2018).
2. V.V. Makarov, L.S. Ksendzenko, N.A. Opanasyuk, A.M Golosov. *Patterns of deformation and fracture highly compressed rocks and massifs*, (Vladivostok, 2014) 250 pp. [In Russian].
3. P. Samui Multivariate Adaptive Regression Spline (Mars) for Prediction of Elastic Modulus of Jointed Rock Mass, 249 (2013).
4. M. Kumar, P. Samui, A Kumar Naithani, Determination of Uniaxial Compressive Strength and Modulus of Elasticity of Travertine using Machine Learning Techniques, **5**, 117 (2013).
5. M. Kumar, G. Bhairevi, P. Samui, Machine Learning Techniques Applied to Uniaxial Compressive Strength of Oporto Granite, **10**, 285 (2014).
6. A. Majdi, M. Beiki, Evolving neural network using a genetic algorithm for predicting the deformation modulus of rock masses, 345 (2010).
7. A. Bahrami, M. Monjezi, K. Goshtasbi, A. Ghazvinian, Prediction of rock fragmentation due to blasting using artificial neural network, 177 (2011)
8. I. Yılmaz, A.G. Yuksek, An Example of Artificial Neural Network (ANN) Application for Indirect Estimation of Rock Parameters, 781 (2008).
9. A.M. Golosov, Development of an acoustic-deformation method for determining precursors of fracture of rock samples under uniaxial compression, (Khabarovsk, 2018). - 150 pp. [In Russian].